

Accurate quantum critical points and nonlocal string order parameters in the spin tetrahedron chain

Zhi-Yong Wu(吴志勇), Kai-Ming Zhang(张凯铭), and Li-Xiang Cen(岑理相)
Citation: Chin. Phys. B, 2025, 34 (**11**): 117502. DOI: 10.1088/1674-1056/ae0c7c
http://cpb.iphy.ac.cn; http://iopscience.iop.org/cpb

What follows is a list of articles you may be interested in

Scaling corrections in driven critical dynamics: Application to the two-dimensional dimerized quantum Heisenberg model

Jing-Wen Liu(刘静雯), Shuai Yin(阴帅), and Yu-Rong Shu(舒玉蓉)
Chin. Phys. B, 2025, 34 (**5**): 057502. DOI: 10.1088/1674-1056/adc672

Semiclassical approach to spin dynamics of a ferromagnetic *S=1* chain

Chengchen Li(李承晨), Yi Cui(崔祎), Weiqiang Yu(于伟强), and Rong Yu(俞榕)
Chin. Phys. B, 2024, 33 (**6**): 067501. DOI: 10.1088/1674-1056/ad3c32

Ground-state phase diagram of the dimerizedspin-1/2 two-leg ladder

Cong Fu(傅聪), Hui Zhao(赵晖), Yu-Guang Chen(陈宇光), and Yong-Hong Yan(鄢永红)
Chin. Phys. B, 2021, 30 (**8**): 087501. DOI: 10.1088/1674-1056/abec31

Emergent O(4) symmetry at the phase transition from plaquette-singlet to antiferromagnetic order in quasi-two-dimensional quantum magnets

Guangyu Sun(孙光宇), Nvsen Ma(马女森), Bowen Zhao(赵博文), Anders W. Sandvik, and Zi Yang Meng(孟子杨)
Chin. Phys. B, 2021, 30 (**6**): 067505. DOI: 10.1088/1674-1056/abf3b8

Absence of magnetic order in dichloro [1,2-bis (diphenylphosphino) ethane] nickel^{2+} single crystal

Shuaiqi Ma(马帅奇), Linlin An(安琳琳), and Xiangde Zhu(朱相德)
Chin. Phys. B, 2021, 30 (**5**): 057501. DOI: 10.1088/1674-1056/abe233

COMPUTATIONAL PROGRAMS FOR PHYSICS

Accurate quantum critical points and nonlocal string order parameters in the spin tetrahedron chain

Zhi-Yong Wu(吴志勇), Kai-Ming Zhang(张凯铭), and Li-Xiang Cen(岑理相)†

Center of Theoretical Physics, College of Physics, Sichuan University, Chengdu 610065, *China*

(Received 16 July 2025; revised manuscript received 25 September 2025; accepted manuscript online 29 September 2025)

The ground-state phase diagram and nonlocal order parameters of an infinite spin tetrahedron chain with inhomogeneous exchange couplings are investigated. It is shown that the phase boundaries of the three phases in the model can be determined precisely, in line with the precision of its ground-state energy. Numerical calculations using the regularized time-evolving block decimation (rTEBD) algorithm yield the locations of the two quantum critical points with an accuracy about 10 digits. Moreover, we explain how to calculate the parity-associated string order for the output wave function obtained through the rTEBD procedure, which not only reveals the presence of long-range correlations but also identifies the symmetry-protected topological order within the intermediate phase of the model.

Keywords: quantum phase transition, time-evolving block decimation algorithm, string order

PACS: 75.10.Jm, 75.10.Pq, 64.70.Tg

DOI: 10.1088/1674-1056/ae0c7c **CSTR:** 32038.14.CPB.ae0c7c

1. Introduction

Quantum phase transitions (QPTs) are remarkable phenomena that account for how quantum many-body systems at extremely low temperatures can exhibit dramatically different properties in response to small changes in microscopic parameters.[1,2] Accurately locating and identifying QPTs has sparked intense research, not only in condensed matter physics but also across various relevant fields. Quantum quench protocols[3–5] have been proposed to detect QPTs, as the occurrence of QPTs leaves distinctive imprints on the evolving state. The corresponding non-analytic behavior at the critical time, known as the dynamical QPT,[6] can be captured through signatures such as the Loschmidt echo.[7–9] Moreover, the sensitivity of QPTs to parameter variations has been exploited for metrological and sensing applications,[10–13] in conjunction with quantum information technology.

Low-dimensional quantum magnets, especially those with strong geometrical frustration, have long attracted interest as they have exchange coupling patterns favoring the existence of competing ground states.[14–17] The spin-$1/2$ chain and ladder systems provide an ideal platform that allows controlled calculations to explore diverse ground-state phase diagrams, including gapless spin liquid states, dimer states, and various ordered states.[18–22] The competing interactions in quasi one-dimensional (1D) mixed-spin $(1/2,1)$ systems have also been studied, with these systems often exhibiting ferrimagnetic long-range order and enriching the range of phases in such systems.[23–26] While the ground-state energy of 1D and quasi 1D spin lattice models is more amenable to numerical investigations thanks to methods like the density matrix renormalization group (DMRG)[27,28] and the infinite time-evolving block decimation (TEBD) algorithm,[29,30] which allow for high precision, accurately locating QPTs for the frustrated systems remains generally challenging and difficult. Note that close to a QPT point, multiple phases may coexist or be nearly degenerate. The critical ground state may not be represented properly by a finite-dimension matrix product state (MPS). As a result, approximate methods such as DMRG and TEBD with truncation of the bond dimension often struggle to pinpoint the transition point, as large amounts of computational resources are needed.

In this paper, we investigate an infinite frustrated magnet of the spin tetrahedron chain previously introduced by Chen *et al.*[31] We focus on quantum critical points in its ground-state phase diagram which comprises three distinct phases: a decoupled state consisting of rung singlets and a Luttinger liquid state, a ferrimagnetic ordered phase arising from the mixed-spin $(1/2,1)$ model with next-nearest neighbor interactions, and an intermediate phase accounting for the mixed-spin $(1/2,1)$ model with diluted triplet rungs. It turns out that the QPT points of the system can be precisely determined, with an accuracy about 10 digits obtained by a regularized TEBD (rTEBD) algorithm,[32] which matches the precision of its ground-state energy. Furthermore, we reveal the existence of nonlocal order parameters with respect to the parity-associated string correlator[33,34] in the gapped ground state of the intermediate phase. It enables us to identify the symmetry-protected topological (SPT) order[35–38] for the gapped phase.

†Corresponding author. E-mail: lixiangcen@scu.edu.cn

© 2025 Chinese Physical Society and IOP Publishing Ltd. All rights, including for text and data mining, AI training, and similar technologies, are reserved.

The rest of the paper is organized as follows. In Section 2, we introduce the spin tetrahedron chain model and describe the structure of its Hamiltonian in the thermodynamical limit. By decomposing the system into a series of reduced models within subspaces, we explain that the QPT points of the model could be accurately determined by combining the numerical calculation and linear fitting approach. Section 3 presents the rTEBD algorithm, detailing its implementation and advantages for infinite quasi 1D lattices. Using this method, we compute the ground-state phase diagram and precisely locate the QPT points separating the decoupled rung-singlet/Luttinger liquid phase, the ferrimagnetic ordered phase, and the intermediate gapped phase. In Section 4, we examine nonlocal order parameters in the intermediate phase, uncovering parity-associated string correlations and demonstrating the presence of SPT order. Finally, the discussion and summary are presented in Section 5.

2. Model and analysis

2.1. Description of the model

We consider the spin-1/2 anti-ferromagnetic Heisenberg model on an infinite tetrahedron chain as shown in Fig. 1(a). The Hamiltonian is characterized by[31]

$$H=\sum_i h_B^{[i]}+v_{i,i+1}, \tag{1}$$

in which $h_B^{[i]}$ $(i=1,\ldots,N\to\infty)$ denotes the "free" Hamiltonian term of every three-site unit cell

$$h_B^{[i]}=J\boldsymbol{S}_{i,1}\cdot(\boldsymbol{S}_{i,2}+\boldsymbol{S}_{i,3})+J_\perp\boldsymbol{S}_{i,2}\cdot\boldsymbol{S}_{i,3} \tag{2}$$

and $v_{i,i+1}=J\sum_{\alpha=1}^{3}\boldsymbol{S}_{i,\alpha}\cdot\boldsymbol{S}_{i+1,1}$ accounts for the inter-block coupling. We have assumed inhomogeneous exchange interactions: $J_\perp\neq J$, where $J_\perp$ indicates the strength of vertical rung (couplings between $\boldsymbol{S}_{i,2}$ and $\boldsymbol{S}_{i,3}$ in every triangle block) and $J>0$ denotes anti-ferromagnetic couplings between $\boldsymbol{S}_{i,1}$ and $\boldsymbol{S}_{i,2(3)}$ and those inter-block interactions, i.e., between $\boldsymbol{S}_{i,\mu}$ $(\mu=1,2,3)$ and $\boldsymbol{S}_{i+1,1}$.

It is direct to observe that the Casimir operators of the total spins on every vertical rung, $(\boldsymbol{S}_{i,2}+\boldsymbol{S}_{i,3})^2\equiv\boldsymbol{t}_i^2$, are conserved: $[\boldsymbol{t}_i^2,H]=0$. The Hamiltonian (1) can be rewritten as

$$\begin{aligned}H=&J\sum_i[\boldsymbol{S}_{i,1}\cdot\boldsymbol{t}_i+(\boldsymbol{S}_{i,1}+\boldsymbol{t}_i)\cdot\boldsymbol{S}_{i+1,1}]\\&+\frac{1}{2}J_\perp\sum_i\left(\boldsymbol{t}_i^2-\frac{3}{2}\right).\end{aligned} \tag{3}$$

According to that the vertical rungs are in singlets or in triplets, the relevant eigenstates of the system are classified by the series of values $t_i=0$ or 1 in corresponding subspaces. Among all possible configurations one needs consider those with a periodic structure in order to find the ground state, as disorder in the configuration will generally increase the energy of the system. That is to say, under the low-energy condition, the Hamiltonian of the tetrahedron chain reduces to a series of (full or sparse) Δ-chain models (see Fig. 1) in the subspaces: $H\to\bigoplus_{q,k}\mathcal{H}_\Delta^{(q,k)}$, where q denotes the size (the number of all singlet and triplet vertical rungs) of the unit cell of the corresponding Δ chain and k indicates the possible internal configurations of the unit cell. Note that a configuration with large-sized unit cells reflects significant local disorder, which consequently raises the energy of the wave function. Thus, it is unnecessary to consider the configuration with excessively large unit cells. In Fig. 1(b), we plot all the configurations of reduced Δ-chain models with $q\leq 3$, recorded as $\mathcal{H}_{r\Delta}$, in which r denotes the ratio of spin triplets in all q vertical rungs. The full Δ chain ($r=1$) consists of N spins with $S=1/2$ on the sites of the lower row and N spins with $t=1$ on the sites of the upper row, respectively. The associated Hamiltonian reads $\mathcal{H}_\Delta=H_\Delta+(1/4)NJ_\perp$, where

$$H_\Delta\equiv J\sum_i[\boldsymbol{S}_i\cdot\boldsymbol{T}_i+(\boldsymbol{S}_i+\boldsymbol{T}_i)\cdot\boldsymbol{S}_{i+1}] \tag{4}$$

with $\boldsymbol{S}_i\equiv\boldsymbol{S}_{i,1}$ and $\boldsymbol{T}_i$ denoting the spin-1 operator (the triplet rung). On the other hand, for the special case of $r=0$, i.e., each rung on the tetrahedron chain forming a singlet state, the Hamiltonian reduces to

$$\mathcal{H}_0=J\sum_i\boldsymbol{S}_i\cdot\boldsymbol{S}_{i+1}-\frac{3}{4}NJ_\perp\equiv H_0-\frac{3}{4}NJ_\perp, \tag{5}$$

where $H_0=J\sum_i\boldsymbol{S}_i\cdot\boldsymbol{S}_{i+1}$ accounts for the conventional spin-1/2 Heisenberg chain and is known to be exactly solvable by the Bethe ansatz method. Similarly, for the cases with $r=2/3,1/2,1/3$, the reduced models are described by sparse Δ chains with rN diluted $t=1$ spins uniformly distributed on the sites of the upper row and the corresponding Hamiltonian

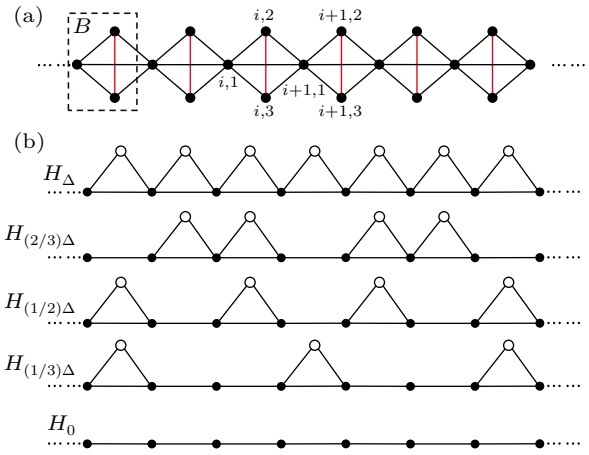


Fig. 1. Schematic picture of the infinite tetrahedron chain and reduced Δ-chain models with respect to various subspaces. (a) The tetrahedron chain and contained three-site unit cells B in which the black and red solid lines represent the exchange interactions with strength J and $J_\perp$, respectively. (b) The series of reduced Δ-chain models $H_{r\Delta}$, with $r=1,2/3,1/2,1/3$ and 0, accounting for the interactions in those subspaces specified by $\mathcal{H}_{r\Delta}$ accordingly. The white and black circles represent spin-1 and spin-1/2 sites, respectively.

$\mathcal{H}_{r\Delta} = H_{r\Delta} + [r-(3/4)]NJ_\perp$. Note that the lowest energy levels of all these reduced $\mathcal{H}_{r\Delta}$'s exhibit a linear dependence on $J_\perp$ (or $J_\perp/J$ with fixed J), suggesting that the QPT points can be identified by finding the intersections of the corresponding straight lines.

2.2. An accurate way to determine quantum critical values for the model

A similar decomposition of the Hamiltonian into the reduced form in the corresponding subspaces is presented in Ref. [31], but for the finite-size tetrahedron chain. Following such description, the phase diagram of the system can then be determined by comparing the ground-state energies of all those sparse and full Δ-chain models $\mathcal{H}_{r\Delta}$. For instance, in the case of $J_\perp/J \gg 1$, it is readily seen that the lowest energy corresponds to all $t_i = 0$, so the ground state of the system (1) is specified by that of $\mathcal{H}_0$, a product of rung singlets and Luttinger liquid ground state of H_0. On the other hand, as $J_\perp \to -\infty$, all the vertical rungs should be in spin triplets so as to minimize the energy. Thus the ground state of the system is determined by that of the full Δ chain $\mathcal{H}_\Delta$.

Interestingly, the linear fitting results in Ref. [31] reveal that there is an intermediate phase between the above two phases, i.e., of $\mathcal{H}_0$ and of $\mathcal{H}_\Delta$. The corresponding ground-state phase is dominated by the half Δ chain $\mathcal{H}_{(1/2)\Delta}$, a doubly degenerate state with alternating spin singlets and triplets on the rungs. However, the conclusion presented in the literature is based on numerical calculations for the finite system. The evidence hence is less rigorous, especially considering that the reference lattice configurations used for comparison therein lack translational invariance. In contrast, we will later confirm this conclusion for the infinite tetrahedron chain. Should the intermediate phase exist, the phase diagram of the model with respect to the coupling strength ratio $\eta \equiv J_\perp/J$ can then be determined by the linear fitting method.

In detail, we record the scaling energy of the "single site" average of every sparse or full Δ-chain model by $\epsilon_{r\Delta} \equiv \langle \mathcal{H}_{r\Delta}\rangle_0/(NJ)$ with $\langle\cdots\rangle_0$ denoting the expectation value over the ground state. For the aforementioned $\mathcal{H}_\Delta$, $\mathcal{H}_{(1/2)\Delta}$, and $\mathcal{H}_0$, there are

$$\begin{cases} \epsilon_\Delta(\eta) = e_\Delta + \frac{1}{4}\eta, \\ \epsilon_{(1/2)\Delta}(\eta) = e_{(1/2)\Delta} - \frac{1}{4}\eta, \\ \epsilon_0(\eta) = e_0 - \frac{3}{4}\eta, \end{cases} \tag{6}$$

respectively, in which the single-site energy $e_{r\Delta}$ is given by $e_{r\Delta} \equiv \langle H_{r\Delta}\rangle_0/N$ with $J = 1$. As a consequence, the critical values, which correspond to intersections of the three straight lines described by Eq. (6) (see also Fig. 2), can be determined simply by

$$\eta_1 = 2(e_{(1/2)\Delta} - e_\Delta), \quad \eta_2 = 2(e_0 - e_{(1/2)\Delta}). \tag{7}$$

That is to say, the precision with which the critical points can be determined could be as high as that achievable for the average ground-state energies e_Δ and $e_{(1/2)\Delta}$ (in view that $e_0 = (1/4) - \ln 2$ is known exactly).

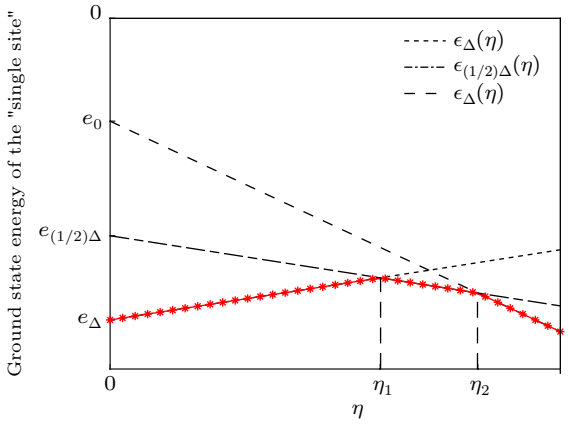


Fig. 2. Ground-state phase diagram of the tetrahedron chain with respect to the parameter $\eta = J_\perp/J$. As the slopes of straight lines $\epsilon_\Delta(\eta)$, $\epsilon_{(1/2)\Delta}(\eta)$ and $\epsilon_0(\eta)$ are known to be $1/4$, $-1/4$ and $-3/4$ [see Eq. (6)], respectively, the critical points $\eta_{1,2}$ can be determined directly by the values of e_Δ, $e_{(1/2)\Delta}$, and e_0 [see Eq. (7)]. Thus the ground-state phase of the system (the red star line) is dominated by that of the full Δ chain $\mathcal{H}_\Delta$ for $\eta < \eta_1$, and by that of the half Δ chain $\mathcal{H}_{(1/2)\Delta}$ for $\eta_1 < \eta < \eta_2$. For the case of $\eta > \eta_2$, the ground state is a product of rung singlets and the Luttinger spin liquid ground state of H_0.

3. Numerical results with the regularized TEBD algorithm

3.1. Brief introduction to the rTEBD algorithm

In the thermodynamic limit, the wave function of 1D quantum many-body systems is represented by an infinite MPS, which consists of a few local matrices that is repeated throughout the infinite chain. The key ingredient of the TEBD algorithm[29,30] and extended time-evolution tensor network state algorithms[39,40] resides in a Trotter–Suzuki splitting of the (imaginary) propagator into a series of local two-site operators so that they can be applied efficiently on the MPS or PEPS repetitively. The rTEBD enhances the infinite TEBD algorithm in two aspects:[32] (1) it partitions the lattice into enlarged blocks (unit cells), thus can be naturally applied to deal with the quasi 1D lattice systems; (2) it employs a regularized factorization of the propagator, which reduces the Trotter error to that of a higher-order Baker–Campbell–Hausdorff (BCH) expansion.

To be specific, let us takes the half Δ-chain model as an example. A partition scheme splitting the lattice into three-spin unit cells (the coarse site Δ's) is shown in Fig. 3(a). The Hamiltonian $H_{(1/2)\Delta}$ of the quasi 1D chain can be expressed as (setting $J = 1$)

$$H_{(1/2)\Delta} = \sum_{j=1}^{N/2} (h_\Delta^{[j]} + v_{j,j+1}^\Delta), \tag{8}$$

in which $h_\Delta^{[j]} = (\boldsymbol{S}_1^{[j]} + \boldsymbol{S}_2^{[j]}) \cdot \boldsymbol{T}^{[j]} + \boldsymbol{S}_1^{[j]} \cdot \boldsymbol{S}_2^{[j]}$ denotes the "free" term of every coarse site and $v_{j,j+1}^{\Delta} = \boldsymbol{S}_2^{[j]} \cdot \boldsymbol{S}_1^{[j+1]}$ accounts for the coupling between them. The rTEBD scheme, named as rTEBD-$(\Delta+\Delta)$ here, can be built by applying the following regularized factorization to the imaginary-time propagator: $U(\tau) = \mathrm{e}^{-\tau H_{(1/2)\Delta}}$:

$$U(\tau) \approx [\bar{U}_{2\Delta}(\tau)]^{\otimes \mathcal{N}} \times [U_{2\Delta}(\tau)]^{\otimes \mathcal{N}}. \tag{9}$$

Here, $\mathcal{N} = (1/4)N$ and $U_{2\Delta}^{[k]}(\tau) = \mathrm{e}^{-\tau h_{2\Delta}^{[k]}}$ in which $h_{2\Delta}^{[k]} = h_\Delta^{[k]} + h_\Delta^{[k+1]} + v_{k,k+1}^{\Delta}$ with $k = 2j-1$. The operator $\bar{U}_{2\Delta}(\tau)$, imposing on every two coarse sites $2j$ and $2j+1$, is constructed through an inward algorithm[41] using either an open or a periodic prescription, e.g., the open one takes the form [see Fig. 3(a)]

$$\bar{U}_{2\Delta}^{[2j]}(\tau) = \mathrm{e}^{-\tau h_{2\Delta}^{[2j]}} \mathrm{e}^{\tau (h_\Delta^{[2j]} + h_\Delta^{[2j+1]})}. \tag{10}$$

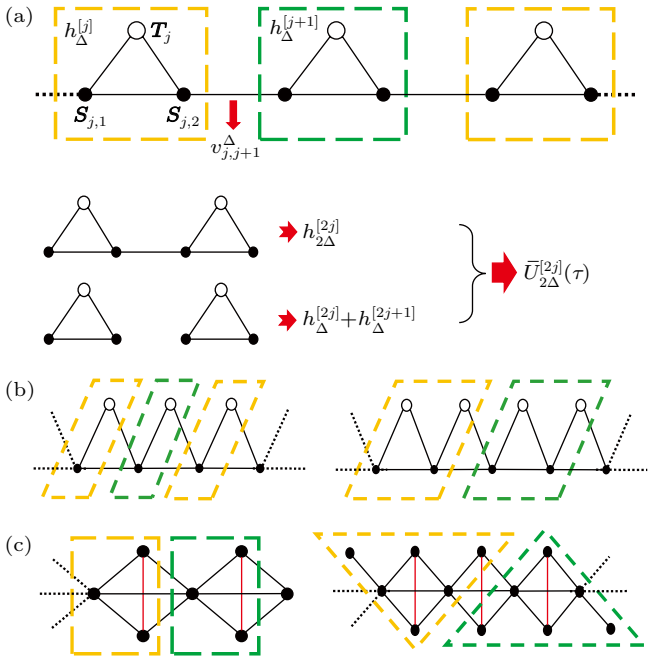


Fig. 3. Partition schemes of the quasi 1D spin lattices and the open prescription in the rTEBD algorithm. (a) Partition of the lattice $H_{(1/2)\Delta}$ into three-site unit cells, being Δ shape with one spin-1 site (white circle) at the upper vertex and two spin-1/2 sites (black circles) at lower vertices. The corresponding open prescription to construct the operator $\bar{U}_{2\Delta}(\tau)$ for rTEBD-$(\Delta+\Delta)$ is illustrated [cf. Eqs. (9) and (10)]. (b) Two different partition schemes responsible for rTEBD-$(2+2)$ and rTEBD-$(4+4)$, in which the lattice model H_Δ is split into two-site or four-site unit cells, respectively. (c) Two partition schemes responsible for rTEBD-$(3+3)$ and rTEBD-$(6+6)$, in which the original tetrahedron chain is split into three-site or six-site unit cells, respectively.

To demonstrate that the factorization of Eq. (9) represents a high-order BCH expansion of the propagator, $U(\tau)$ can be rewritten as

$$U(\tau) = \mathrm{e}^{-\tau H_{(1/2)\Delta}} \mathrm{e}^{\tau \sum_k h_{2\Delta}^{[k]}} \times \mathrm{e}^{-\tau \sum_k h_{2\Delta}^{[k]}}. \tag{11}$$

Then one is led to notice the equivalence between the multiplication of the first two factors and those operators of Eq. (10) under a finite-order BCH expansion, i.e.,

$$\mathrm{e}^{-\tau H_{(1/2)\Delta}} \mathrm{e}^{\tau \sum_k h_{2\Delta}^{[k]}} \approx [\bar{U}_{2\Delta}(\tau)]^{\otimes \mathcal{N}}. \tag{12}$$

Firstly, it is readily seen that under the lowest-order (1th-order) BCH expansion, both left and right hands of Eq. (12) reduce to $\otimes_{j=1}^{\mathcal{N}} \mathrm{e}^{-\tau v_{2j,2j+1}^{\Delta}}$, hence the regularized factorization in Eq. (9) recovers the usual Suzuki–Trotter formula.[42] Moreover, for the 2nd-order BCH expansion, both left and right hands involve only a commutator between $v_{2j,2j+1}^{\Delta}$ and $h_\Delta^{[2j]} + h_\Delta^{[2j+1]}$, so the equality remains to be true. Whereas, for the 3rd or much higher-order expansions, the nesting commutators between $H_{(1/2)\Delta}$ and $v_{2j,2j+1}^{\Delta}$ in the left hand of the above equation will break the range of the local building block, hence the factorization of Eq. (9) causes an error $\sim O(\tau^3)$ to the current system.

Following the infinite TEBD scheme, the local operators obtained in Eq. (9) are applied in sequence on the target MPS which can be updated accordingly. In the limit that the inverse temperature $\beta = M\tau \to \infty$, there is $U(\beta) \propto |\psi_0\rangle\langle\psi_0|$ and the ground state $|\psi_0\rangle$ can then be obtained by applying the operators of Eq. (9) iteratively on a randomly chosen initial state. The average ground-state energy per "coarse site" can be obtained through the rTEBD algorithm via $e_{\mathrm{g}} = \langle h_\Delta^{[j]} + v_{j,j+1}^{\Delta} \rangle_0$, which relates to the aforementioned $e_{(1/2)\Delta}$ [cf. Eq. (6)] by $e_{(1/2)\Delta} = \frac{1}{2} e_{\mathrm{g}}$. In Figs. 3(b) and 3(c) we depict further partition schemes for the full Δ chain and the infinite tetrahedron chain, with which the corresponding algorithms, i.e, rTEBD-$(2+2)$ and rTEBD-$(4+4)$ for the former, and rTEBD-$(3+3)$ and rTEBD-$(6+6)$ for the latter, can be built.

3.2. Phase diagram and accurate phase boundaries of the tetrahedron chain

With the rTEBD algorithm, we are able to check whether there exists the intermediate phase, the ground state with alternating spin singlets and triplets on the vertical rungs, which is predicted in Ref. [31] through exact diagonalization on finite-size systems. In detail, we perform the rTEBD-$(3+3)$ and rTEBD-$(6+6)$ [cf. Fig. 3(c)] to achieve the ground state of the model (1) with different values of $\eta = J_\perp/J$. The values of the angular momentum of two adjacent rung spins $\langle \boldsymbol{t}_i^2 + \boldsymbol{t}_{i+1}^2 \rangle_0$ are computed and shown in Fig. 4 (plotted as a function of η). The existence of three different phases is confirmed, that is, full triplet rungs specified by $\langle \boldsymbol{t}_i^2 + \boldsymbol{t}_{i+1}^2 \rangle_0 = 4$, full singlet rungs by $\langle \boldsymbol{t}_i^2 + \boldsymbol{t}_{i+1}^2 \rangle_0 = 0$, and alternating singlet and triplet rungs specified by $\langle \boldsymbol{t}_i^2 + \boldsymbol{t}_{i+1}^2 \rangle_0 = 2$. In the vicinity of the two transition points, the numerical results become unstable due to their strong dependence on the randomly chosen initial state. This is because that the phases are nearly degenerate at QPTs, making the corresponding phase boundary difficult to determine precisely through such calculations.

Notwithstanding, the former analysis [see Eqs. (6) and (7) in Subsection 2.2] reveals that to determine the critical points

$\eta_{1,2}$ one needs only calculate the average ground-state energies of the full and half Δ-chain models H_Δ and $H_{(1/2)\Delta}$, i.e., the values of e_Δ and $e_{(1/2)\Delta}$. The performance of the rTEBD-$(\Delta+\Delta)$ on the model $H_{(1/2)\Delta}$, specifically the rapid convergence of the iterative process, suggests that the model has a gapped ground state. Its energy is readily determined to an accuracy of over 10 digits with the bond dimension $\chi \lesssim 32$ and Trotter step $\tau \gtrsim 0.004$: $e_{(1/2)\Delta} = -0.9327043509(2)$. As demonstrated in Table 1, an extrapolation with the bond dimension $\chi > 32$ will not affect the first ten digits of $e_{(1/2)\Delta}$ here, and only serves to refine the data beyond the 11th digit of it. Consequently, the phase boundary of $\mathcal{H}_0$ and $\mathcal{H}_{(1/2)\Delta}$ can be determined with the same accuracy: $\eta_2 = 0.9791143407(1)$. On the other hand, the algorithm on the model H_Δ needs more iteration to reach convergence due to the presence of competing states with respect the spin frustration. In Fig. 5, we depict the curves of e_Δ achieved by the rTEBD-$(2+2)$ with bond dimensions $\chi = 8, 10, 16, 24$. The Trotter step τ is gradually reduced to 10^{-4} so that the associated Trotter error is negligible comparing with that of the bond truncation. As expected, the rTEBD-$(4+4)$ improves the results by accounting for more correlations and reducing the truncation error caused by the approximation of the mean-field-like environment. By performing rTEBD-$(4+4)$, we obtain $e_\Delta = -1.29354613(4)$ with $\chi = 24$. Subsequently, the location of the critical point is obtained as $\eta_1 = 0.72168356(7)$.

Table 1. Ground-state energy of the half Δ-chain model $H_{(1/2)\Delta}$ obtained by the algorithm rTEBD-$(\Delta+\Delta)$.

$e_{(1/2)\Delta}$	$\tau = 0.008$	$\tau = 0.004$	$\tau = 0.002$
$\chi = 16$	−0.932704338183	−0.932704338187	−0.932704338187
$\chi = 24$	−0.932704350511	−0.932704350513	−0.932704350513
$\chi = 28$	−0.932704350900	−0.932704350901	−0.932704350902
$\chi = 32$	−0.932704350915	−0.932704350916	−0.932704350916

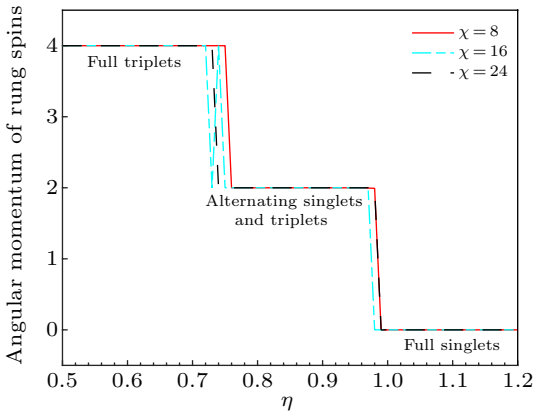


Fig. 4. The values of the angular momentum of two adjacent rung spins $\langle \boldsymbol{t}_i^2 + \boldsymbol{t}_{i+1}^2 \rangle_0$ of the tetrahedron chain obtained by the rTEBD-$(3+3)$ algorithm starting from randomly chosen initial states with bond dimensions $\chi = 8$, 16, and 24. The results exhibit distinctly the existence of three different phases. The algorithm of rTEBD-$(6+6)$ yields almost the same results but the areas of uncertainty near the two transition points become slightly narrow.

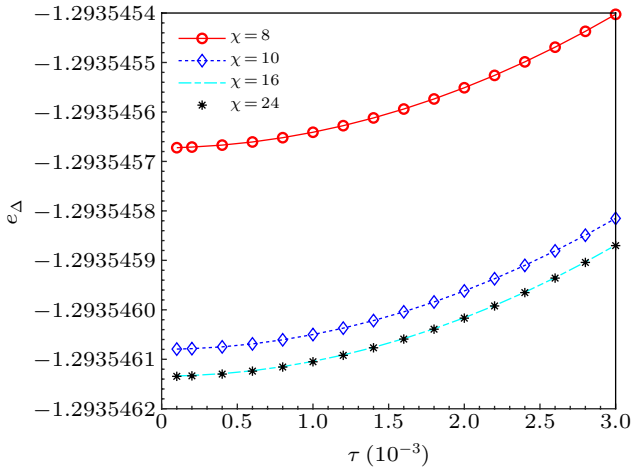


Fig. 5. The average ground-state energies e_Δ of the model H_Δ achieved by the rTEBD-$(2+2)$ with different sizes of Trotter step τ and various bond dimension χ.

3.3. Lowest levels in subspaces with respect to two sparse Δ chains

As an additional verification, we use the rTEBD algorithm to calculate the ground-state energies of the two sparse Δ-chain models $H_{(1/3)\Delta}$ and $H_{(2/3)\Delta}$. The corresponding average values are obtained as $e_{(1/3)\Delta} \approx -0.73535$ and $e_{(2/3)\Delta} \approx -1.04506$ with $\chi = 18$ (setting $J = 1$). The lowest levels $\epsilon_{(1/3)\Delta}(\eta)$ and $\epsilon_{(2/3)\Delta}(\eta)$ in the corresponding subspaces specified by $\mathcal{H}_{(1/3)\Delta}$ and $\mathcal{H}_{(2/3)\Delta}$ are plotted in Fig. 6 in terms of the parameter $\eta = J_\perp/J$. Both curves lie above the aforementioned phase curves of Fig. 2 across all three regions: $\eta < \eta_1$, $\eta_1 < \eta < \eta_2$, and $\eta > \eta_2$, thus justifying the proposed ground-state phase diagram.

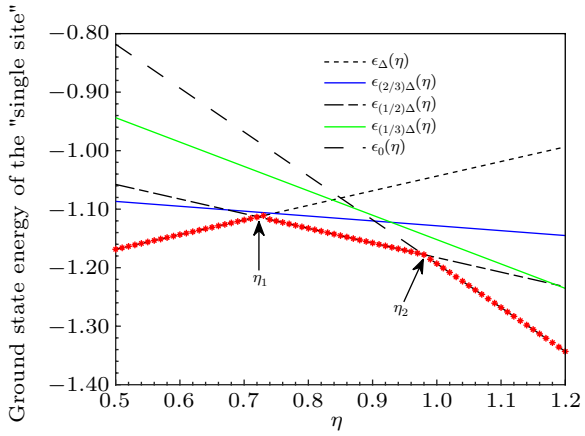


Fig. 6. The lowest levels $\epsilon_{(1/3)\Delta}(\eta)$ and $\epsilon_{(2/3)\Delta}(\eta)$ of $\mathcal{H}_{(1/3)\Delta}$ and $\mathcal{H}_{(2/3)\Delta}$, in contrast with the phase diagram determined by $\epsilon_\Delta(\eta)$, $\epsilon_{(1/2)\Delta}(\eta)$, and $\epsilon_0(\eta)$. The curves are verified to be above the ground-state phase curves across all the regions.

4. Nonlocal order parameter in the intermediate phase of the tetrahedron chain

4.1. String-order correlators in the gapped intermediate phase

The ground state of the tetrahedron chain over $\eta < \eta_1$, i.e., that of the Hamiltonian H_Δ in Eq. (4), is believed to

possess ferrimagnetic order just like the original mixed-spin $(1/2,1)$ system with only nearest-neighbor interactions.[31] This is confirmed by our rTEBD algorithm which reveals that in the full Δ chain there is $|\langle S^z\rangle_0| \approx 0.0725(0)$ for the spin $1/2$ and $\langle T^z\rangle_0 \approx -3.0644\langle S^z\rangle_0$ for the spin 1 (with the bond dimension $\chi = 24$). On the other hand, numerical calculation shows that all the ground-state average of the spins $S^\mu_{j,1}$, $S^\mu_{j,2}$, and T^μ_j ($\mu = x,y,z$) of the model $H_{(1/2)\Delta}$ are zero. It indicates that the intermediate phase of the tetrahedron chain has neither ferromagnetic nor anti-ferromagnetic order. Despite the absence of conventional long-range order, we show below that this gapped intermediate phase exhibits a sort of nonlocal string order. The latter was originally introduced by Den Nijs and Rommelse[43] and was shown to be a common feature of the Affleck–Kennedy–Lieb–Tasakimodel model (AKLT)[44] and the Haldane-like phase with a valence-bond solid structure.[45–50]

In detail, we resort to the parity-associated string order correlator introduced in Ref. [33]

$$\mathrm{SO_P}(O_1,O_2) \equiv \lim_{j'-j\to\infty} \langle O_1^{[j]} \mathcal{P}^{(l)} O_2^{[j']}\rangle_0, \tag{13}$$

in which $O_{1,2}$ are two local observables and the parity operator $\mathcal{P}^{(l)}$ acts on the consecutive $l = j'-j-1$ unit cell Δ's between the boundary ones j and j'. Note that while the full translation symmetry is slightly broken in the MPS obtained by the rTEBD, spatial reflection symmetry and two-Δ translation invariance are preserved. As a result, the output of the ground state of the model $H_{(1/2)\Delta}$ [the one in Eq. (8) with $\mathcal{N} = N/2$ Δ cells] can be represented by

$$|\psi_0\rangle = \sum_{\{s_\Delta^{[j]}\}} \mathrm{Tr}\left[A^{s_\Delta^{[1]}} B^{s_\Delta^{[2]}} \cdots A^{s_\Delta^{[\mathcal{N}-1]}} B^{s_\Delta^{[\mathcal{N}]}}\right] \left|s_\Delta^{[1]} \cdots s_\Delta^{[\mathcal{N}]}\right\rangle, \tag{14}$$

in which $s_\Delta^{[j]}$ denotes the spin degree of freedom of the jth Δ. Due to the spatial reflection symmetry, the representative matrices satisfy $(A^{s_\Delta})^{\mathrm{T}} = B^{s_\Delta}$, or there exists a similarity transformation X such that

$$(A^{s_\Delta})^{\mathrm{T}} = X B^{s_\Delta} X^{-1}, \quad (B^{s_\Delta})^{\mathrm{T}} = X A^{s_\Delta} X^{-1}. \tag{15}$$

Here, we assume that the MPS $|\psi_0\rangle$ is generally not in the canonical form and X is an invertible matrix (doesn't have to be unitary). By choosing the spin-1 operators T^μ as the boundary observables, the string order parameter is characterized as

$$\mathrm{SO_P}(T_B^\mu, T_A^\mu) = \lim_{l\to\infty} \frac{\langle \Psi_\mathrm{L}| E_{T_B^\mu} E_{\mathcal{P}^{(2l)}} E_{T_A^\mu} |\Psi_\mathrm{R}\rangle}{\lambda_\mathrm{M}^{l+1}}, \tag{16}$$

in which λ_M accounts for the maximal eigenvalue of the transfer matrix $E_{BA} \equiv E_B E_A$ with $E_Q = \sum_{s_\Delta} (Q^{s_\Delta})^* \otimes Q^{s_\Delta}$ ($Q = A, B$). The bra $\langle \Psi_\mathrm{L}|$ and ket $|\Psi_\mathrm{R}\rangle$ denote the corresponding left and right eigenvectors of E_{BA} with respect to λ_M. The the parity-associated transfer matrix $E_{\mathcal{P}^{(2l)}}$ is defined as

$$\begin{aligned} E_{\mathcal{P}^{(2l)}} &= \sum_{s_\Delta^{[1]},\cdots,s_\Delta^{[2l]}} (A^{s_\Delta^{[1]}} \cdots B^{s_\Delta^{[2l]}})^* \otimes A^{s_\Delta^{[2l]}} \cdots B^{s_\Delta^{[1]}} \\ &= \sum_{s_\Delta^{[1]},\cdots,s_\Delta^{[2l]}} (A^{s_\Delta^{[1]}} \cdots B^{s_\Delta^{[2l]}})^* \otimes (A^{s_\Delta^{[1]}} \cdots B^{s_\Delta^{[2l]}})^{\mathrm{T}} \\ &\equiv (E_{AB}^l)^{\mathrm{T}_2}, \end{aligned} \tag{17}$$

where $E_{AB} = E_A E_B$ and we have assumed $(A^{s_\Delta})^{\mathrm{T}} = B^{s_\Delta}$ herein. The observable associated $E_{T_A^\mu}$ and $E_{T_B^\mu}$ are specified by

$$E_{T_Q^\mu} = \sum_{s_\Delta, s'_\Delta} \langle s_\Delta | T_Q^\mu | s'_\Delta\rangle (Q^{s_\Delta})^* \otimes Q^{s'_\Delta}. \tag{18}$$

In the limit $l \to \infty$, there is $E_{\mathcal{P}^{(2l)}} \to \lambda_\mathrm{M}^l (|\Phi_\mathrm{R}\rangle\langle\Phi_\mathrm{L}|)^{\mathrm{T}_2}$, where $|\Phi_{\mathrm{L(R)}}\rangle$ denotes the left (right) eigenvector of E_{AB} with respect to the eigenvalue λ_M. Consequently, one obtains

$$\mathrm{SO_P}(T_B^\mu, T_A^\mu) = \lambda_\mathrm{M}^{-1} \langle \Psi_\mathrm{L}| E_{T_B^\mu} (|\Phi_\mathrm{R}\rangle\langle\Phi_\mathrm{L}|)^{\mathrm{T}_2} E_{T_A^\mu} |\Psi_\mathrm{R}\rangle. \tag{19}$$

For the case that $(A^{s_\Delta})^{\mathrm{T}} \neq B^{s_\Delta}$ but there is an invertible X satisfying Eq. (15), the string order $\mathrm{SO_P}(T_B^\mu, T_A^\mu)$ is achievable similarly but that the quantity $E_{\mathcal{P}^{(2l)}}$ in Eq. (16) is given by $E_{\mathcal{P}^{(2l)}} = (\tilde{E}_{AB}^l)^{\mathrm{T}_2}$ in which

$$\begin{aligned} \tilde{E}_{AB} &= \sum_{s_\Delta, s'_\Delta} (A^{s_\Delta} B^{s'_\Delta})^* \otimes (B^{s_\Delta})^{\mathrm{T}} (A^{s'_\Delta})^{\mathrm{T}} \\ &= (I \otimes X) E_{AB} (I \otimes X^{-1}). \end{aligned} \tag{20}$$

Thus one needs only to replace the factor $(|\Phi_\mathrm{R}\rangle\langle\Phi_\mathrm{L}|)^{\mathrm{T}_2}$ in Eq. (19) by $I \otimes (X^{-1})^{\mathrm{T}} (|\Phi_\mathrm{R}\rangle\langle\Phi_\mathrm{L}|)^{\mathrm{T}_2} I \otimes X^{\mathrm{T}}$. In the practical calculation, one needs not to know the detailed form of the invertible matrix X but can utilize the expression of $\tilde{E}_{AB}$ in the first line of Eq. (20) directly. Our numerical calculation displays that the string order is independent of the orientation μ and the value is approximately $\mathrm{SO_P}(T_B^\mu, T_A^\mu) \approx 0.0193$.

4.2. Detecting the phase factor of the symmetry-protected topological phase

Interestingly, string order parameters have been used to distinguish SPT phases, which are the topological class of gapped phases that arise in the presence of certain symmetry, e.g., the on-site rotation, spatial reflection or time-reversal symmetry.[35–38] SPT phases are known to host a variety of fascinating topological properties, such as the Haldane phase in 1D spin chains and the quantum spin Hall effect in 2D systems.[51,52] Since there are no local bulk properties that can be measured to distinguish an SPT phase, it is highly nontrivial to identify different SPT phases physically.

For the spatial inversion symmetry, the topological property is classified by the phase factor $X^{-1}X^{\mathrm{T}} = \pm 1$, i.e., the

similarity matrix X being either symmetric or anti-symmetric. The latter is obtained from two facts:[35,36] (1) $X^{-1}X^{\mathrm{T}} = \mathrm{e}^{\mathrm{i}\phi}$ since $AB = (X^{-1})^{\mathrm{T}}XABX^{-1}X^{\mathrm{T}}$, (2) $X = (X^{\mathrm{T}})^{\mathrm{T}} = X\,\mathrm{e}^{2\mathrm{i}\phi}$, so $\mathrm{e}^{\mathrm{i}\phi} = 1$ or -1. To detect the phase factor $\mathrm{e}^{\mathrm{i}\phi}$ for the wave function, one can take the observable $O_{1,2}$ in Eq. (13) to be the identity operator. It gives rise to

$$\mathrm{SO_P} \equiv \lim_{l\to\infty} \frac{\langle\psi_0|\mathcal{P}^{(2l)}|\psi_0\rangle}{\langle\psi_0|\psi_0\rangle} = \lim_{l\to\infty} \frac{\langle\Phi_{\mathrm{L}}|(\tilde{E}_{AB}^{l})^{\mathrm{T}_2}|\Phi_{\mathrm{R}}\rangle}{\lambda_{\mathrm{M}}^{l}}. \quad (21)$$

In Ref. [34], it was shown that, using the canonical MPS form, the sign of the above $\mathrm{SO_P}$ measures the phase factor $\mathrm{e}^{\mathrm{i}\phi} = \pm 1$ and thus distinguishes between topological phases. The demonstration in that work relies on an assumption that the similarity transformation [cf. Eq. (15)] is unitary, which makes it somewhat limited in scope. Meanwhile, as the quantity is independent of a concrete MPS representation, it is surely valid to detect the phase factor of the wave function $|\psi_0\rangle$ in a non-canonical form.

To achieve the explicit expression of the string order $\mathrm{SO_P}$ for a general MPS representation, let us introduce the following notations:

$$\xi_{ij} = \langle ij|\Phi_{\mathrm{R}}\rangle, \quad \zeta_{ij} = \langle ij|\Phi_{\mathrm{L}}\rangle, \quad (22)$$

that is, the matrix ξ (ζ) is defined by setting the two indices i and j of $|\Phi_{\mathrm{R}}\rangle$ ($|\Phi_{\mathrm{L}}\rangle$) as its row and column indices, respectively. According to Eq. (15), one has

$$E_{AB}^{\mathrm{T}} = X^* \otimes X E_{AB} (X^*)^{-1} \otimes X^{-1}. \quad (23)$$

So the left eigenvector $|\Phi_{\mathrm{L}}\rangle$ of E_{AB} (i.e., the right one of $E_{AB}^{\dagger}$) relates to $|\Phi_{\mathrm{R}}\rangle$ via $|\Phi_{\mathrm{L}}\rangle = X \otimes X^*|\Phi_{\mathrm{R}}^*\rangle$. It indicates that ξ and ζ satisfy

$$\zeta = X\xi^* X^{\dagger}. \quad (24)$$

Consequently, the string order $\mathrm{SO_P}$ is shown to be

$$\begin{aligned} \mathrm{SO_P} &= \langle\Phi_{\mathrm{L}}|I \otimes (X^{-1})^{\mathrm{T}}(|\Phi_{\mathrm{R}}\rangle\langle\Phi_{\mathrm{L}}|)^{\mathrm{T}_2} I \otimes X^{\mathrm{T}}|\Phi_{\mathrm{R}}\rangle \\ &= \mathrm{Tr}(\zeta^* X^{-1}\zeta^{\dagger}\xi X^{\mathrm{T}}\xi^{\mathrm{T}}) \\ &= \mathrm{Tr}[(X^{\mathrm{T}}X^{-1})^*(\zeta^*\xi^{\mathrm{T}})^2] \\ &= \pm\mathrm{Tr}[(\zeta^*\xi^{\mathrm{T}})^2], \end{aligned} \quad (25)$$

where we have used the relation (24) to obtain the third equality and the one $X^{\mathrm{T}} = \pm X$ to obtain the last equality. In the canonical representation, the right eigenvector of the transfer matrix E_{AB} takes the form of $\xi_{ij} = \langle ij|\Phi_{\mathrm{R}}\rangle = \delta_{ij}$. Thus the result of Eq. (25) reduces further to $\mathrm{SO_P} = \pm\mathrm{Tr}[(XX^{\dagger})^2]$, wherein $\mathrm{Tr}(XX^{\dagger}) = 1$ according to $\langle\Phi_{\mathrm{L}}|\Phi_{\mathrm{R}}\rangle = 1$. For the ground state of $H_{(1/2)\Delta}$, the phase factor turns out to be $\mathrm{e}^{\mathrm{i}\phi} = 1$ and the value of $\mathrm{SO_P}$ yielded by our rTEBD is $\mathrm{SO_P} \approx 0.8729$.

5. Discussion and conclusion

The high-precision QPT points obtained above enable potential quantum sensing protocols. Suppose that the system of the tetrahedron chain is prepared in $|\psi_0(\eta_a)\rangle$, the ground state of the Hamiltonian $\tilde{H}(\eta) \equiv H/J$ with the parameter $\eta = \eta_a$. Its time evolution is driven with a Hamiltonian $\tilde{H}(\eta_b)$ where the parameter $\eta_b = \eta_a + \delta$ with δ denoting a small perturbation. For quenches across the quantum critical point, e.g., $\eta_a < \eta_2 < \eta_b$, the dynamical QPT can be detected by the nonanalytic behavior of Loschmidt echo $L(\delta, t) \equiv |\langle\psi_0(\eta_a)|\,\mathrm{e}^{-\mathrm{i}t\tilde{H}(\eta_b)}|\psi_0(\eta_a)\rangle|^2$. The potential sensing scheme could be exploited to measure extremely weak interactions, i.e., $\delta \gtrsim 10^{-10}$, which is on the same order as the precision of the value of η_2.

To summarize, we have studied the spin-1/2 antiferromagnetic Heisenberg model on an infinite tetrahedron chain using both theoretical analysis and numerical calculation. The ground-state phase diagram of the model, featuring three distinct phases, is characterized by both the ground-state energy and the angular momentum of vertical rungs. By utilizing the rTEBD algorithm, we have demonstrated that the QPT points separating the decoupled rung-singlet/Luttinger liquid phase, the ferrimagnetic ordered phase, and the intermediate gapped phase, can be precisely determined in line with the model's ground-state energy, with locations given by the coupling parameter ratios $J_{\perp}/J = 0.9791143407(1)$ and $0.72168356(7)$.

We have also explored the hidden long-range order in the model, revealing the nonlocal string correlations in the intermediate phase with respect to spatial inversion symmetry. This parity-associated string order not only confirms the presence of long-range correlations but also provides a physical distinction of the SPT phase. The combination of high-precision critical-point determination and the characterization of SPT order provides a comprehensive understanding of the model's rich phase diagram. Further investigation into the analogy between the current SPT phase and the AKLT model, as well as the emergence of edge modes under open boundary conditions, would be a subject of interest. Also, the methodology developed here, particularly the regularization technique in the rTEBD, holds promise for investigating the complex behavior of quasi 1D frustrated quantum lattice systems. In addition, the precise quantum criticality achieved has the potential to serve as a sensitive probe for precision measurements, advancing experimental techniques in quantum sensing and quantum enhanced metrology.

Program availability

The source code of this study is available from the corresponding author upon reasonable request.

Acknowledgment

Project supported by the National Natural Science Foundation of China (Grant No. 12471443).

References

[1] Sachdev S 2011 *Quantum Phase Transitions* (Cambridge: Cambridge University Press)
[2] Carr L D E 2010 *Understanding Quantum Phase Transitions* (Boca Raton: Taylor and Francis)
[3] Sadler L E, Higbie J M, Leslie S R, Vengalattore M and Stamper-Kurn D M 2006 *Nature* **443** 312
[4] Lian H L 2012 *Chin. Phys. C* **36** 479
[5] Dağ C B, Wang Y, Uhrich P, Na X and Halimeh J C 2023 *Phys. Rev. B* **107** L121113
[6] Heyl M, Polkovnikov A and Kehrein S 2013 *Phys. Rev. Lett.* **110** 135704
[7] Gorin T, Prosen T, Seligman T H and Znidaric M 2006 *Phys. Rep.* **435** 33
[8] Quan H T, Song Z, Liu X F, Zanardi P and Sun C P 2006 *Phys. Rev. Lett.* **96** 140604
[9] Jafari R and Johannesson H 2017 *Phys. Rev. Lett.* **118** 015701
[10] Fernández-Lorenzo S and Porras D 2017 *Phys. Rev. A* **96** 013817
[11] Rams M M, Sierant P, Dutta O, Horodecki P and Zakrzewski J 2018 *Phys. Rev. X* **8** 021022
[12] Heugel T L, Biondi M, Zilberberg O and Chitra R 2019 *Phys. Rev. Lett.* **123** 173601
[13] Garbe L, Bina M, Keller A, Paris M G A and Felicetti S 2020 *Phys. Rev. Lett.* **124** 120504
[14] Lacroix C, Mendels P and Mila F 2011 *Introduction to Frustrated Magnetism* (Berlin: Springer)
[15] Balents L 2010 *Nature* **464** 199
[16] Marić V, Giampaolo S M and Franchini F 2022 *Phys. Rev. B* **105** 064408
[17] Ghosh S, Singh R R P and Kumar M 2025 *Phys. Rev. B* **111** 045115
[18] Nersesyan A A, Gogolin A O and Ebßler F H L 1998 *Phys. Rev. Lett.* **81** 910
[19] Mikeska H J and Luckmann C 2008 *Phys. Rev. B* **77** 054405
[20] Derzhko O, Krokhmalskii T and Richter J 2010 *Phys. Rev. B* **82** 214412
[21] Furuya S C and Giamarchi T 2014 *Phys. Rev. B* **89** 205131
[22] Maiti D, Dey D and Kumar M 2018 *J. Mag. Mag. Mater.* **446** 170
[23] Kolezhuk A K, Mikeska H J and Yamamoto S 1997 *Phys. Rev. B* **55** R3336
[24] Ivanov N B 2009 *Condens. Matter Phys.* **12** 435
[25] Chandra V R, Ivanov N B and Richter J 2010 *Phys. Rev. B* **81** 024409
[26] Jiang J J, Liu Y J, Tang F and Yang C H 2012 *Phys. B* **407** 4810
[27] White S R 1992 *Phys. Rev. Lett.* **69** 2863
[28] White S R 1998 *Phys. Rep.* **301** 187
[29] Vidal G 2007 *Phys. Rev. Lett.* **98** 070201
[30] Orús R and Vidal G 2008 *Phys. Rev. B* **78** 155117
[31] Chen S, Wang Y, Ning W Q, Wu C and Lin H Q 2006 *Phys. Rev. B* **74** 174424
[32] Cen L X 2022 arXiv:2208.03436v1 [cond-mat.str-el]
[33] Cen L X 2009 *Phys. Rev. B* **80** 132405
[34] Pollmann F and Turner A M 2012 *Phys. Rev. B* **86** 125441
[35] Pollmann F, Turner A M, Berg E and Oshikawa M 2018 *Phys. Rev. B* **81** 064439
[36] Chen X, Gu Z C and Wen X G 2011 *Phys. Rev. B* **83** 035107
[37] Schuch N, Pérez-García D and Cirac I 2011 *Phys. Rev. B* **84** 165139
[38] Chen X, Gu Z C and Wen X G 2011 *Phys. Rev. B* **84** 235128
[39] Jordan J, Orús R, Vidal G, Verstraete F and Cirac J 2008 *Phys. Rev. B* **101** 250602
[40] Jiang H C, Weng Z Y and Xiang T 2008 *Phys. Rev. Lett.* **101** 090603
[41] Cen L X 2018 *Ann. Phys.* **397** 151
[42] Suzuki M 1990 *Phys. Lett. A* **146** 319
[43] den Nijs M and Rommelse K 1989 *Phys. Rev. B* **40** 4709
[44] Affleck I, Kennedy T, Lieb E H and Tasaki H 1987 *Phys. Rev. Lett.* **59** 799
[45] Kennedy T and Tasaki H 1992 *Phys. Rev. B* **45** 304
[46] Hida K 1992 *Phys. Rev. B* **45** 2207
[47] Greiter M, Rachel S and Schuricht D 2007 *Phys. Rev. B* **75** 060401
[48] Gong S S and Su G 2008 *Phys. Rev. B* **78** 104416
[49] Perez-Garcia D, Wolf M M, Sanz M, Verstraete F and Cirac J I 2008 *Phys. Rev. Lett.* **100** 167202
[50] Fu C, Zhao H, Chen Y G and Yan Y H 2021 *Chin. Phys. B* **30** 087501
[51] Hasan M Z and Kane C L 2010 *Rev. Mod. Phys.* **82** 3045
[52] Qi X L and Zhang S C 2011 *Rev. Mod. Phys.* **83** 1057